Top Organomet Chem (2016) 56: 67–90
DOI: 10.1007/3418_2015_138

Published online: 26 July 2015

The Effects of Ancillary Ligands on Metal–Carbon Bond Strengths as Determined by C–H Activation

William D. Jones

Abstract The activation of C–H bonds by oxidative addition in about 30 different substrates has been examined with three closely related metal species, [Tp′RhL], where L = CNneopentyl, PMe_3, and $P(OMe)_3$. Kinetic studies of the reductive elimination of R–H provided data to ascertain the relative metal–carbon bond strengths for a wide range of compounds. Trends in these bond strengths reveal that there are two classes of C–H substrates: parent hydrocarbons and substituted methanes. DFT calculations are used to support the observed trends, and some generalizations are made by comparison to other metal systems.

Keywords Bond strengths · Kinetics · Oxidative addition · Reductive elimination · Rhodium · Thermodynamics

Contents

W.D. Jones (✉)
Department of Chemistry, University of Rochester, Rochester, NY 14627, USA
e-mail: jones@chem.rochester.edu

1 Introduction

Carbon–hydrogen bond activation by transition metals has found its way to becoming an important aspect of organic synthesis. Metals have been found to break C–H bonds and then participate in follow-up reactions, oftentimes insertions of olefins or alkynes, that permit functionalization of a substrate or the formation of fused-ring systems. As this chemistry is developed, it is clear that selectivity in C–H bond activation is a critical issue that must be controlled to make a given functionalization reaction valuable.

In this chapter, we will present a summary of results that have been reported over the last 25 years with a transition metal complex that activates a wide variety of C–H bonds. As this chemistry developed, additional insight has been obtained that permitted further extensions of the work that have led to a deeper understanding of the factors that influence metal–carbon bond strengths. These bond strengths play an important role in determining the selectivity in reactions such as regioselective olefin insertions, so it is important to be able to predict how the formation of one bond vs. another will affect the thermodynamics. The importance of these factors will be revealed, and the effects of ancillary or "spectator" ligands on metal–carbon bond strengths will also be quantitatively analyzed and interpreted. This is all possible because the unsaturated metal fragment [Tp′RhL] where L = CNR, PMe_3, or $P(OMe)_3$ has proven to be very reactive toward a wide variety of C–H bonds, allowing the necessary comparisons to be made.

2 Hydrocarbon Activation by [Tp′Rh(CNR)]

We first reported that the 16-electron rhodium fragment [Tp′Rh(CNR)] where CNR = neopentyl isocyanide could activate hydrocarbon C–H bonds by irradiation of the carbodiimide precursor in benzene [1]. 366 nm irradiation of the yellow complex **1** led to the colorless phenyl hydride product in good yield. The quantum yield was determined to be 1.0 ± 0.3, which is higher than for many other organometallic photoprecursors [2–6]. Compound **1** is readily prepared by the reaction of phenyl azide with the $Tp'Rh(CNR)_2$.

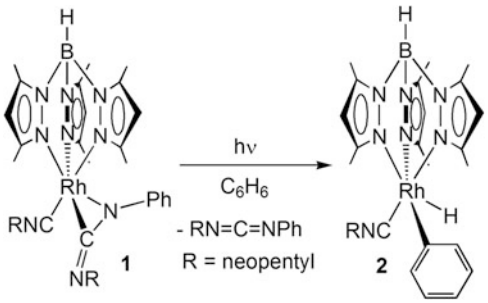

(1)

Benzene loss from **2** occurs upon warming to 80°C, with $\Delta G^{\ddagger} = 29.8$ kcal/mol in C_6D_6. The 16-electron fragment that apparently forms is rapidly trapped by the solvent to give **2**-d_6. The true mechanism, however, is one in which the benzene is displaced. If neopentyl isocyanide is added to **2**, a bimolecular reaction occurs to generate Tp′Rh(CNR)$_2$. The rate is first order in [CNR] at low isocyanide concentrations but zero order in [CNR] at high isocyanide concentrations, which is consistent with a pre-equilibrium between **2** and the η^2 complex (κ^2-Tp′)Rh(η^2-C_6H_6)(CNR) followed by associative substitution of the benzene at a square planar coordinatively unsaturated intermediate (Eq. 2). Further evidence for reversible formation of an η^2-benzene intermediate came from the observation of scrambling in the complex Tp′Rh(CNR)(C_6D_5)H. The hydride appears in all five locations on the phenyl group at the same rate, implying that the η^2-C_6D_5H complex is fluxional. Rh-phenyl rotation is hindered at room temperature, and at low T, five distinct phenyl resonances can be observed in the ^{1}H NMR spectrum [7].

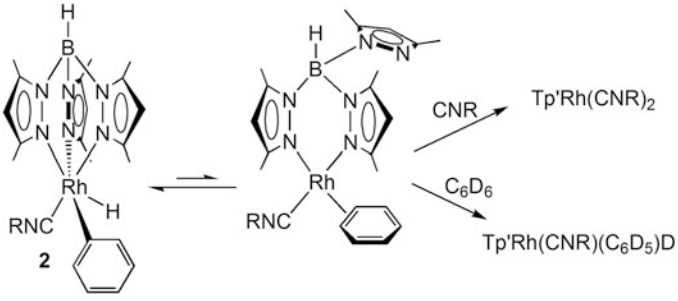

(2)

Complex **1** was found to activate a wide variety of hydrocarbons, including propane, pentane, cyclohexane, cyclopentane, methane, mesitylene, isobutene, and *t*-butylethylene [8, 9]. For linear hydrocarbons, a kinetic preference was observed for the exclusive activation of the C–H bonds of the terminal methyl groups. The activation of secondary C–H bonds was only observed when no other primary C–H bonds were available (e.g., cyclohexane, cyclopentane, cyclopropane [10]). With mesitylene, both aromatic and benzylic C–H bonds were cleaved. These observations were interpreted in terms of initial coordination of the hydrocarbon C–H bond to the 16-electron rhodium fragment, followed by rapid migration along the chain to

the end methyl group, where oxidative cleavage was rapid. This hypothesis was supported by experiments using deuterium-labeled alkyl deuterides. By monitoring the rates at which the deuterium appeared in the α and distal positions of the alkyl group vs. dissociation, the relative rates could be established as $k_{\text{C–H cleavage}} > k_{\text{migration}} > k_{\text{dissociation}}$ (Eq. 3) [11].

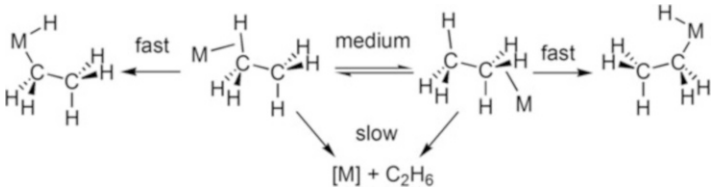

(3)

Further evidence for the intermediacy of alkane complexes came from studies of the reductive elimination of methane from Tp′Rh(CNR)(Me)H, **3**. Here, the rate of reaction with C_6D_6 to produce **2**-d_6 was found to be dependent on the concentration of C_6D_6 in inert C_6F_6 solvent. As with the reaction with isocyanide in Eq. 2, the rate was first order in $[C_6D_6]$ at low concentrations but less than first order at higher $[C_6D_6]$. These observations were treated in terms of a reversible equilibrium between **3** and an η^2-methane complex that then underwent bimolecular displacement by benzene. The reaction also shows a "solvent kinetic isotope effect," with the rate being faster in C_6H_6 than in C_6D_6 ($k_{C_6H_6}/k_{C_6D_6} = 1.08$). Since the rate-determining step involves bimolecular reaction with benzene, the rate is slightly different with C_6D_6 vs. C_6H_6 [12].

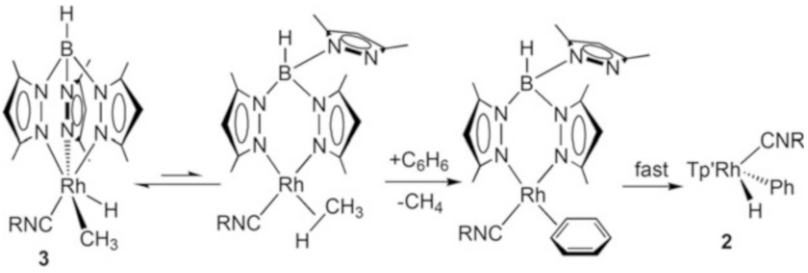

(4)

Terminal alkynes also add to [Tp′Rh(CNR)]. Irradiation of the carbodiimide complex **1** in neat 1-alkyne leads to the activation of the sp C–H bond. In cases where other "activatable" C–H bonds were presented, competitive C–H activation at these positions was observed. For example, *t*-butylacetylene and trifluoromethyl acetylene give exclusively alkynyl hydride products, whereas 1-octyne and trimethylsilylacetylene also give products resulting from methyl group activation. In both of the latter cases, the sp^3 C–H activation products are unstable and convert to the terminal alkynyl products at room temperature after a few days (Scheme 1). Similarly, the activation of arylalkynes leads to mixtures of sp and sp^2 C–H activation products. The unsaturated fragment [Tp′Rh(CNR)] was prepared either

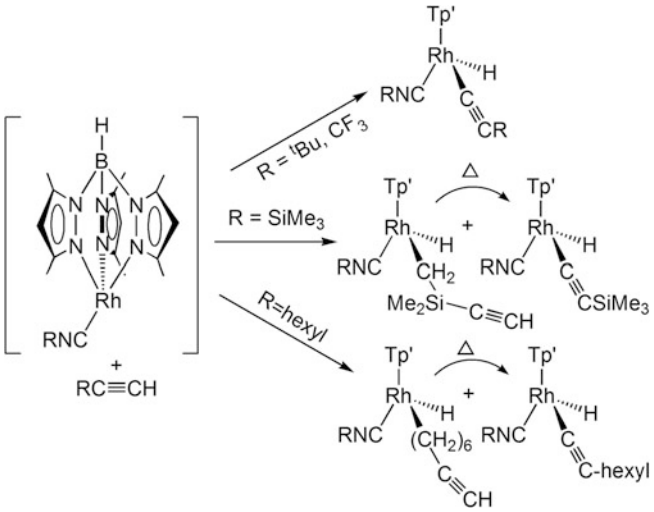

Scheme 1 Reactions of [Tp′Rh(CNR)] with terminal alkynes

by irradiation of **1** or by reductive elimination of methane from **3** in the presence of the alkyne [13].

The fragment [Tp′Rh(CNR)], prepared from irradiation of **1** or reductive elimination of methane from **3**, was found to react with a wide variety of substituted methanes. In each case, exclusive activation of the methyl C–H bond was observed, giving products of the type Tp′Rh(CNR)(CH_2X)H (X = *m*-xylyl, 2-propenyl, OMe, O^{t}Bu, CN, Cl, F, CF_3, C≡CMe, or C(=O)Me, Eq. 5) [14]. Difluoromethane also underwent clean oxidative addition of the C–H bond, but trifluoromethane proved unreactive, perhaps due to steric hindrance from the fluorines.

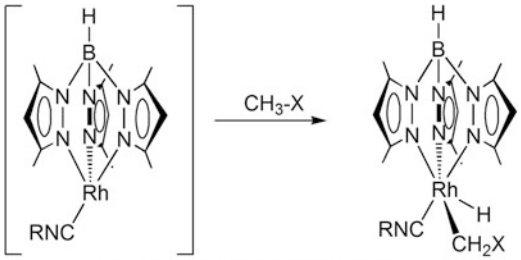

(5)

Irradiation of **1** in a series of linear nitriles was also examined and found to give terminal methyl activation products as the dominant species in all cases. Traces (~5%) of α-cyano C–H activation could be seen with propionitrile and butyronitrile (Eq. 6).

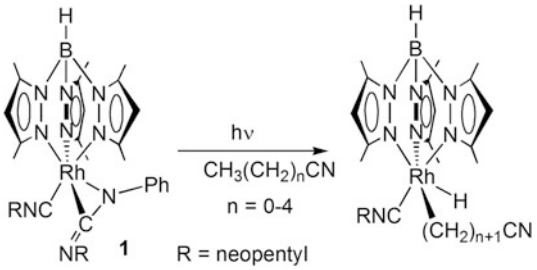

(6)

3 Thermodynamic Determination of Rhodium–Carbon Bond Strengths in Tp′Rh(CNR)(R)H

Through our studies of the above C–H activation reactions, we have found that we could do additional kinetic experiments to provide thermodynamic information on the stability of the various derivatives. These complexes all vary only in the hydrocarbyl group attached to rhodium – the spectator ligands are kept constant – so that relative bond strengths can be extracted from these studies.

The method employed uses three kinetic measurements to obtain the basic data needed to establish relative thermodynamic stabilities. The first two measurements needed to compare two complexes is the rate at which they reductively eliminate hydrocarbon. This is obtained by dissolving the pure compound in benzene-d_6 and then measuring the rate of the first-order reductive elimination. This rate constant can then be converted to a barrier height using the Eyring equation. The third kinetic measurement needed is to perform a competition between the two substrate hydrocarbons when they react with the [Tp′Rh(CNR)] fragment. This is accomplished by irradiation a solution of **1** in a 1:1 molar ratio of the two substrates. The ratio of the products gives the difference in the two barrier heights for C–H activation. The experiments are summarized in Scheme 2 for benzene vs. *t*-butylethylene, and the thermodynamic analysis is shown in Fig. 1.

From the two barrier heights for reductive elimination, combined with the kinetic selectivity, one can obtain the driving force ΔG^0 for the exchange of benzene for *t*-butylethylene in Tp′Rh(CNR)(R)H as shown in Fig. 1. This driving force has both enthalpic and entropic contributions. The enthalpic contributions depend on the relative Rh–C bond strengths (D_{rel}(Rh–C)) and the relative C–H bond strengths ($D_{R2–H} - D_{R1–H}$) in the bonds that are being broken and formed. The entropic contributions largely cancel out, since most of the molecule is the same on both sides of the reaction. There is one important entropic contribution that should be considered, however, and that is to account for the number of hydrogens that are available for activation.

In the present example, benzene has six hydrogens that can react, whereas *t*-butylethylene has only one hydrogen that can react (only the *trans* isomer is formed). Therefore, benzene is six times more likely to react compared to

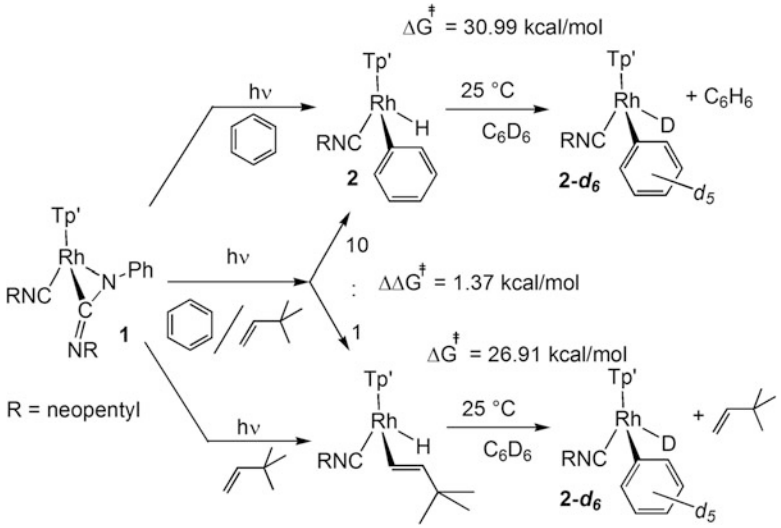

Scheme 2 Three kinetics experiments that allow determination of the driving force

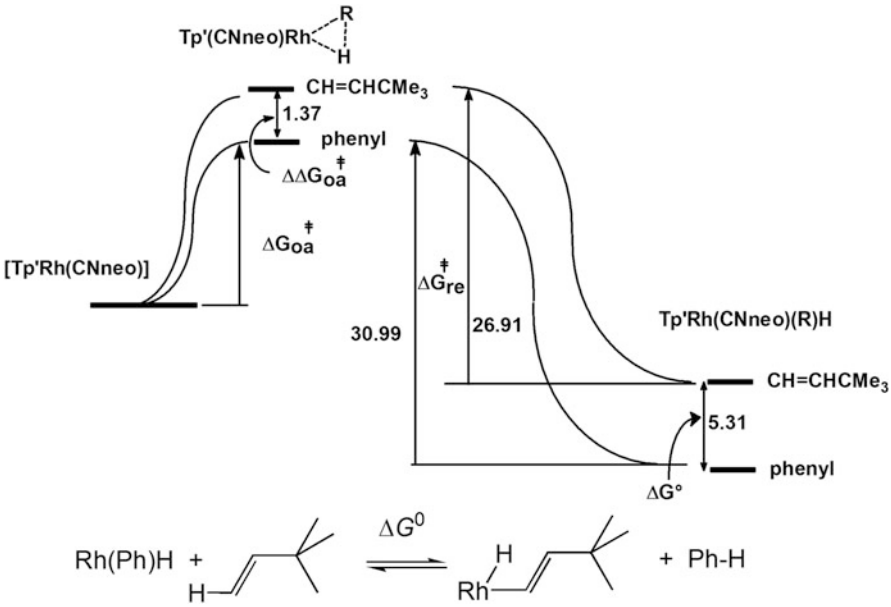

Fig. 1 Thermodynamic analysis of R–H activation equilibrium from the results of three kinetic experiments. Energies are in kcal mol^{-1}

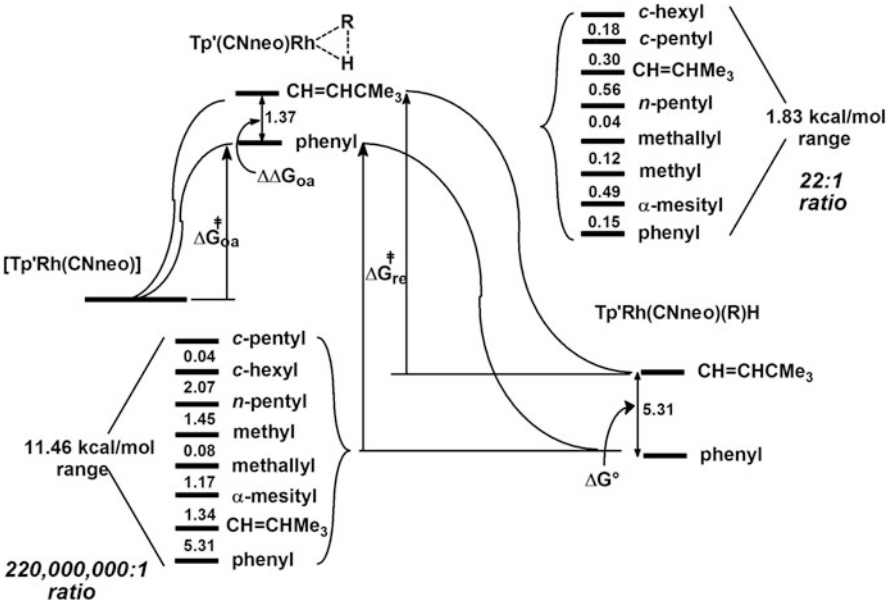

Fig. 2 Thermodynamic analysis of R–H activation equilibrium for several hydrocarbons. Reproduced with permission of the ACS from Jones and Wick [9]

t-butylethylene, and this statistical difference amounts to an entropic contribution to ΔG^0. Equation 7 summarizes how these terms combine for any two hydrocarbons to give the relative metal–carbon bond strength, D_{rel}(Rh–C), from the free energy of reaction:

$$D_{\text{rel}}(\text{Rh}-\text{C}) = \Delta G^0 - [D_{\text{R2}-\text{H}} - D_{\text{R1}-\text{H}}] - RT\ln(\#\text{H}_2/\#\text{H}_1) \qquad (7)$$

This analysis can be applied to all of the hydrocarbon activations discussed thus far, some of which are summarized in Fig. 2. The only requirement is that the C–H activation must give a single product and that the reductive elimination must cleanly give **2**-d_6. If the reductive elimination leads to a rearranged product, then Eq. 7 cannot be used. For example, the activation of cyclopropane leads to the C–H oxidative addition product. However, reductive elimination in C_6D_6 does not give **2**-d_6 but rather produces the metallocyclobutane. Therefore, cyclopropane does not appear in this scheme.

At this point, it is worth commenting on these hydrocarbon activations. First, from the competition experiments, all of the hydrocarbons are activated with similar barriers – that is, the $\Delta\Delta G^{\ddagger}$ only spans 1.8 kcal/mol, which corresponds to a 22:1 ratio at 25°C. This is because in the rate-determining step, the substrate is coordinating to the [Tp′Rh(CNR)] fragment via its C–H bond, and all of the hydrocarbons have similar binding affinities. For aromatic substrates, the arene can bind through its π-system, and this is why benzene and mesitylene are the

fastest substrates to be activated. After this, the kinetic selectivity largely follows steric accessibility to the C–H bond. The range for thermodynamic preference spans a much larger range, 220 million:1 or 11.5 kcal/mol. It is also noteworthy that the most preferred product is the one in which the strongest C–H bond has been broken, the phenyl hydride. This thermodynamic preference for breaking the strongest C–H bond can only be accounted for by the formation of an even more favorable rhodium–phenyl bond. It is the strength of the metal–carbon bond that is formed that drives these equilibria, not the strength of the C–H bond that must be broken. These are product driven equilibria, so the focus on the C–H bond strength to predict favorability is not warranted.

While all of the substrates discussed above are not shown in Fig. 2, the same analysis can be performed with all of them (alkynes, substituted methanes). One caveat that we encountered was that many of these substituted derivatives proved to be very stable. Loss of alkane from the *n*-pentyl hydride complex has a half-life of about an hour at 25°C. Methane loss from **3** has a half-life of about 5 h. Loss of benzene from **2**, however, is extremely slow (months), and therefore, the rate of benzene reductive elimination at 25°C was determined by extrapolation from the rate at higher temperatures. The Eyring plot of ln(*k*/T) vs. 1/T gave activation parameters for reductive elimination of benzene $\Delta H^{\ddagger} = 37.8$ (1.1) kcal/mol and $\Delta S^{\ddagger} = 23$ (3) e.u., which can be used to calculate the rate at other temperatures. As mentioned above, the substituted derivatives are much more stable. Reductive elimination of the alkynyl hydrides was examined at 100°C, as was the elimination of many of the substituted methyl derivatives. In these cases, the rate of benzene elimination was calculated from the Eyring parameters at the same temperature as that where the rate of reductive elimination was measured, so that the barriers could be directly compared as in Fig. 2. The determination of ΔG^0 for all substrates allows Eq. 7 to be used to determine relative metal–carbon bond strengths for these compounds. Table 1 summarizes these data, giving $\Delta\Delta G^{\ddagger}$, ΔG^0, and D_{rel}(Rh–C) for all substrates.

With D_{rel}(Rh–C) now available for all substrates, the data can be compared visually by plotting D_{rel}(Rh–C) vs. the C–H bond strength of the substrate. Figure 3 shows the resulting plot. The data fall into two classes of substrates. The parent hydrocarbon data are shown in blue, with the M–C_{sp} bonds being strongest and then the M–C_{sp2}, followed by the M–C_{sp3}. The line has a slope of 1.4, indicating that the range of metal–carbon bond strengths is about 40% greater than the range of carbon–hydrogen bond strengths. The data for the substituted methanes is shown in red. It is parallel with a slope of 1.4 also but is offset vertically by about 7 kcal/mol. This offset reflects the fact that the metal–carbon bonds are about 7 kcal/mol stronger than what you would expect based upon the strength of the C–H bond that is being broken. Also, while chloro and fluoro substituents are seen to strengthen the metal–methyl bond, all of the other substituents actually *weaken* the metal–methyl bond. This is actually to be expected, as bond strengths are based on homolysis, and these radicals are all stabilized by resonance. The unexpected 7 kcal/mol "increase" in bond strength is believed to be attributable to a greater ionic contribution to the metal–carbon bond with these substituents on the α-carbon.

Table 1 Kinetic and thermodynamic data for Tp′Rh(CNneopentyl)(R)H complexes

R	D(C–H)[a]	$\Delta\Delta G_{oa}^{\ddagger}$ vs. PhH	$\Delta G_{re}^{\ddagger}$	T_{re}(R–H)	ΔG^0 vs. PhH	#H	D_{rel}(M–C)
Ph-	112.9	0	30.95	296	0	6	0.0
t-Butylvinyl-	111.1	1.36	26.91	295	5.47	1	−6.2
Methyl-	105.0	0.70	23.52	296	8.17	4	−15.8
n-Pentyl-	100.2	0.79	22.43	296	9.35	6	−22.1
c-Pentyl-	95.6	1.78	21.18	296	11.59	10	−29.2
c-Hexyl-	99.5	1.80	21.40	296	11.39	12	−25.2
$CF_3C{\equiv}C$-	*135.4*[a]	0.75	30.10	373	−0.13	1	23.7
n-HexylC≡C-	*131.0*[a]	1.19	30.39	373	0.02	1	19.1
$Me_3SiC{\equiv}C$-	*131.6*[a]	0.62	32.50	373	−2.66	1	22.4
$Me_3CC{\equiv}C$-	*131.4*[a]	0.96	30.83	373	−0.65	1	20.2
PhC≡C-	*133.2*[a]	0.50	31.53	373	−1.81	1	23.2
p-$CF_3C_6H_4C{\equiv}C$-	*127.8*[a]	−0.09	31.83	373	−2.70	1	18.7
p-$MeOC_6H_4C{\equiv}C$-	*122.7*[a]	0.29	30.78	373	−1.27	1	12.1
-C_2H_4CN	*103.0*[a]	1.26	25.47	299	6.71	3	−16.2
-C_3H_6CN	*101.3*[a]	1.17	23.64	299	8.45	3	−19.6
-C_4H_8CN	*101.2*[a]	1.04	22.88	299	9.09	3	−20.4
-$C_5H_{10}CN$	*101.2*[a]	1.04	22.38	299	9.58	3	−20.9
-CH_2CN	94.8	1.48	31.36	373	−0.66	3	−17.0
-$CH_2C(Me){=}CH_2$	89.1	0.74	23.92	296	7.81	6	−31.6
α-Mesityl-	89.4	0.13	24.49	296	6.63	9	−30.4
-$CH_2C{\equiv}CCH_3$	90.7	0.44	26.98	340	3.44	6	−25.6
-$CH_2C(O)CH_3$	96.0	0.73	27.71	340	3.00	6	−19.9
-CH_2O^tBu	93.0	0.84	25.43	340	5.39	3	−24.9
-CH_2OCH_3	96.1	0.48	26.24	340	4.22	6	−21.0
-CH_2F	101.3	0.81	28.48	340	2.31	3	−13.5
-CHF_2	103.2	2.33	30.36	373	1.19	2	−10.2
-CH_2Cl	100.1	0.14	27.90	353	1.92	3	−14.3
-C_6F_5[b]	116.5	1.92	36.81	412	−6.57	1	11.2
-CH_2CF_3	106.7	1.63	27.90	340	3.71	3	−9.5

Terminal C–H bond strengths *in italics* for alkynes and nitriles were calculated using DFT; B3LYP/6-31G**

[a]Energies are in kcal mol^{-1}

[b]From Evans et al. [15]

For comparison with the experimental values, we have also calculated these same bond strength data using DFT with Tp′Rh(CNMe)(R)H as a model, with methylisocyanide replacing neopentylisocyanide. A plot of calculated relative Rh–C bond strengths vs. C–H bond strengths with these substrates also shows two distinct linear correlations with slopes of 1.59 and 1.46 for the two analogous sets of compounds (Fig. 4). While there is generally good agreement with the observed experimental trends in Rh–C bond strengths, DFT overestimates the range of Rh–C bond strengths by 10–15%.

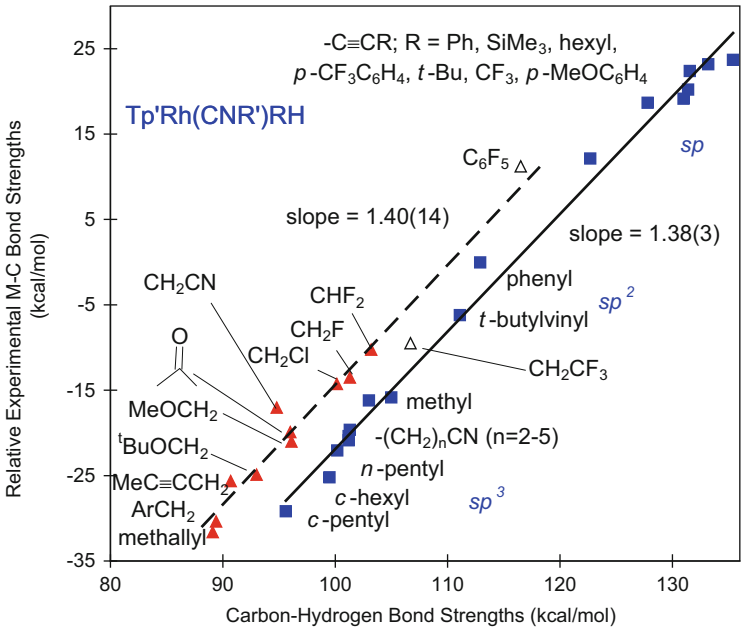

Fig. 3 Plot of relative experimental M–C bond strengths vs. C–H bond strengths. The *solid line* is fit to the hydrocarbons and aliphatic nitriles $-(CH_2)_n-CN$ ($n = 2–5$) (*blue filled box*, $y = 1.376x - 159.5$), and the *dashed line* is fit to the $-CH_2X$ substrates and $-CHF_2$ (*red filled triangle*, $y = 1.4024x - 154.6$). Also shown are $-C_6F_5$ and $-CH_2CF_3$ (Δ), which are not included in either fit. Experimental C–H bond strengths were used for all substrates except the alkynes and nitriles other than acetonitrile. Alkyne and nitrile C–H bond strengths were calculated (B3LYP) since experimental values are unavailable or have large errors [13]. The vertical separation of the lines at $D_{C-H} = 100$ kcal mol^{-1} is 7.5 kcal mol^{-1}. Reproduced with permission of the ACS from Jiao et al. [14]

4 Hydrocarbon Activation by [Tp′Rh(PMe$_3$)]

In order to investigate the effect of the ancillary ligands on the metal–carbon bond strengths, we also examined the reactivity of the fragment [Tp′Rh(PMe$_3$)] with hydrocarbons and substituted methyl derivatives. Here, the strongly electron-donating PMe$_3$ ligand replaces the electron-withdrawing neopentyl isocyanide ligand in the above studies and was anticipated to have a significant effect on the bond strengths.

To generate the 16-electron fragment, Tp′Rh(PMe$_3$)H$_2$ (**4**) was used as a photochemical precursor of the reactive intermediate [16, 17]. Irradiation of **4** in a variety of hydrocarbons led to the formation of oxidative addition products of the type Tp′Rh(PMe$_3$)(R)H (R = α-mesityl, *tert*-butylvinyl, CH_2O^tBu, $CH_2C{\equiv}CMe$, $CH_2C(=O)CH_3$, pentyl, cyclopentyl) along with a small amount of by-products Tp′Rh(PMe$_3$)$_2$ and Tp′Rh(PMe$_3$)R$_2$. The latter are formed as a result of photolysis of the product(s). As an alternative, Tp′Rh(PMe$_3$)MeH (**5**) was prepared by the

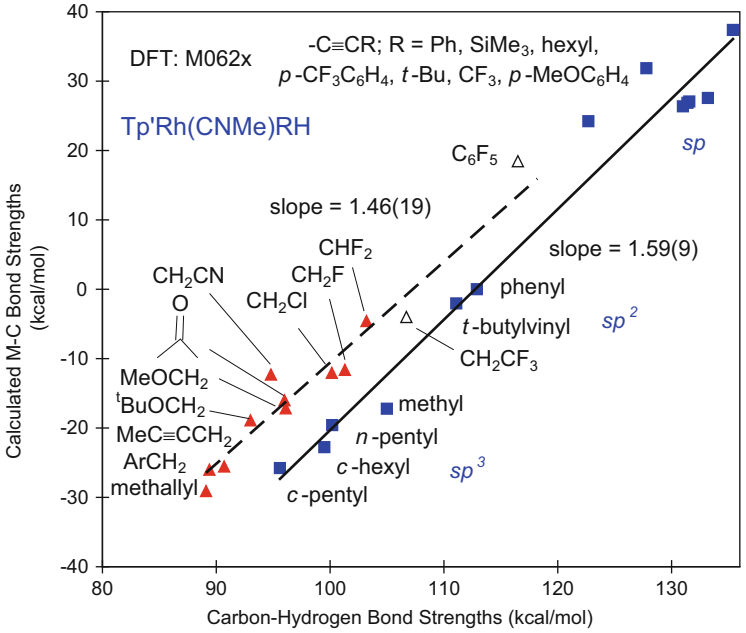

Fig. 4 DFT-calculated plot of relative M–C bond strengths vs. C–H bond strengths for Tp′Rh(CNMe)(R)H. The *lower line* is fit to the hydrocarbons (*blue filled box*, $y = 1.593x - 179.6$), and the *upper line* is fit to the $-CH_2X$ and CHF_2 substrates (*red filled triangle*, $y = 1.457x - 156.2$). Data for C_6F_5H and CH_3CF_3 activation is also shown (Δ), but not included in the fits. M062X method and basis set 6–31g** for first row atoms and pseudopotentials, additional functions optimized by Stuttgart group for atoms beyond the second row (see [13] for details on the choice of method). Experimental C–H bond strengths were used for all substrates except the alkynes. Alkyne C–H bond strengths were calculated (B3LYP) since experimental values are unavailable or have large errors [13]. The vertical separation of the lines at $D_{C-H} = 100$ kcal mol^{-1} is 9.7 kcal mol^{-1}. Reproduced with permission of the ACS from Jiao et al. [14]

reaction of Tp′Rh(PMe_3)MeCl with Cp_2ZrH_2. Loss of methane occurs rapidly at 30°C ($\tau_{1/2} = 35$ min), giving rise to an alternate thermal source of [Tp′Rh(PMe_3)]. During the isolation of **5**, some methane loss and activation of the THF solvent used in the synthesis produced variable quantities of Tp′Rh(PMe_3)(tetrahydrofuranyl)H, which is also a labile source of [Tp′Rh(PMe_3)]. Using **5**, many hydrocarbon and substituted methyl products could be prepared (Scheme 3) [18].

Reaction of mesitylene with **5** gave only the product of benzylic C–H activation, unlike the reaction with **1** which gave a 3:1 mixture of benzylic/aromatic C–H activation. The isonitrile ligand appears to induce less crowding at the metal center. As with **1**, CF_3H proved unreactive. Once again, steric inaccessibility of the C–H bond is believed to be responsible.

Irradiation of dihydride **4** in neat terminal alkyne led to C–H activation products, but the lengthy photolysis times led to decomposition products with many of the acetylenes. Methyl hydride **5** proved to be a good precursor for the activation of

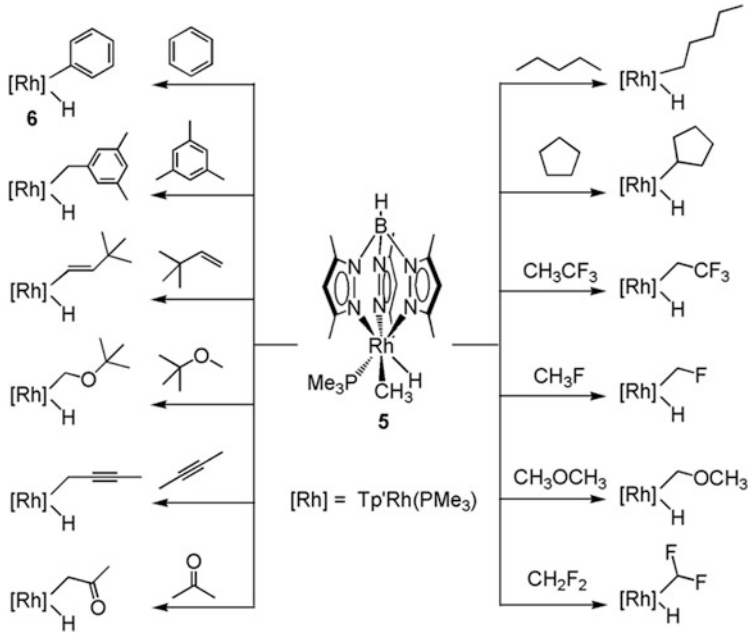

Scheme 3 Reactions of $Tp'Rh(PMe_3)$ with hydrocarbon substrates

terminal alkynes to give products of the type $Tp'Rh(PMe_3)(C{\equiv}CR)H$ ($R = {}^tBu$, $SiMe_3$. *n*-hexyl, *p*-$MeOC_6H_4$, CF_3, Ph, *p*-$CF_3C_6H_4$). In the latter three cases, competitive formation of the π-bound acetylene complex was also observed. Heating these samples to 140°C for several hours resulted in their complete conversion to the alkynyl hydride products (Eq. 8). These alkynyl hydride products proved to be very stable, as they could be chromatographed in air on the benchtop and the X-ray crystal structures of many of them could be obtained without derivatization [18].

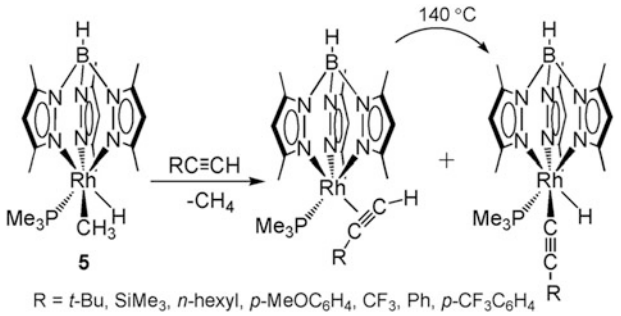

(8)

5 Thermodynamic Determination of Rhodium–Carbon Bond Strengths in Tp′Rh(PMe$_3$)(R)H

As was done previously, the kinetics of reductive elimination, combined with kinetic competition data, were used to obtain rhodium–carbon bond strengths with [Tp′Rh(PMe$_3$)] as the metal fragment. Thermolysis of each compound in C_6D_6 at 30°C was found to follow first-order reductive elimination kinetics, giving Tp′Rh(PMe$_3$)(C_6D_5)D (**6-*d*$_2$**). The only exception was the 2-butynyl hydride Tp′Rh(PMe$_3$)($CH_2C{\equiv}CCH_3$)H, which gave the η^2-butyne complex as confirmed by X-ray crystallography. This complex could therefore not be employed in the thermodynamic analysis. In comparison with the earlier case with Tp′Rh (neopentyl)($CH_2C{\equiv}CCH_3$)H, the elimination of 2-butyne cleanly led to the formation of **2-*d*$_6$**. Apparently the stronger donor PMe$_3$ allows for significant stabilization of the π-bound alkyne complexes.

Some of the compounds underwent reductive elimination far too slowly at 30°C for convenient measurement (e.g., alkynes), and therefore, they were conducted at elevated temperatures (140°C). In addition, since **6-d$_2$** is unstable at this temperature, C_6F_5H was added to trap the metal fragment following reductive elimination. To compare these barriers to those of the reductive elimination of **6**, the temperature dependence of the rate of elimination for **6** in C_6D_6 was measured, giving activation parameters $\Delta H^{\ddagger} = 32.6 \pm 3.3$ kcal mol^{-1} and $\Delta S^{\ddagger} = 10.9 \pm 0.2$ kcal mol^{-1} K^{-1}. Using these data, the barrier heights could be compared at the same temperature.

Kinetic competitions between a substrate and C_6H_6 were accomplished by irradiation of a solution of **4** in a mixture of the two substrates. The samples were irradiated for only a short time to avoid problems arising from secondary photolysis of the products. The ratio of the two products could be easily determined by ^{1}H NMR spectroscopy, giving the value for $\Delta\Delta G^{\ddagger}$. Competition data for methane was measured vs. pentane and then referred to benzene using the competition between pentane and benzene: $k_{\mathrm{PhH}}/k_{\mathrm{CH_4}} = \left(k_{\mathrm{PhH}}/k_{\mathrm{pentane}}\right)\left(k_{\mathrm{pentane}}/k_{\mathrm{CH_4}}\right)$.

As described above for [Tp′Rh(CNneopentyl)], the analysis of the data in Table 2 as in Fig. 1 and using Eq. 7 allows the determination of D_{rel}(Rh–C) for a large number of substrates. These Rh–C bond strengths can be plotted vs. the corresponding C–H bond strengths to give the overall trend as shown in Fig. 5. As before two trends clearly emerge. The first trend is seen joining the unsubstituted hydrocarbons with a slope of 1.54(4). This compares to the value seen with CNneopentyl as the ancillary ligand of 1.38(3). The effect of replacing the strong isocyanide π-acceptor with the strong PMe$_3$ σ-donor is to increase the slope of the line. This corresponds to a "stretching out" of the range of Rh–C bond strengths with the better σ-donor ligand; i.e., the PMe$_3$ derivative shows a wider range of selectivity. The second trend seen is in the methyl-substituted derivatives Rh–CH_2X. Again, a parallel line is observed with a slope of 1.71(8), which compares to the slope seen with L = CNneopentyl of 1.40(14). The line is offset vertically by about 8 kcal/mol, very similar to the values seen with L = CNneopentyl. The range

Table 2 Kinetic and thermodynamic data for Tp′Rh(PMe_3)(R)H complexes

R	D(C–H)[a]	$\Delta\Delta G_{oa}^{\ddagger}$ vs. PhH	$\Delta G_{re}^{\ddagger}$	T_{re}(R–H)	ΔG^0 vs. PhH	#H	D_{rel}(M–C)
Ph-	112.9	0	29.34	303	0.00	6	0.0
t-Butylvinyl-	111.1	0.83	27.99	303	2.18	1	−2.9
Methyl-	105.0	0.49	22.58	303	7.25	4	−14.9
n-Pentyl-	100.2	0.47	21.00	282	9.04	6	−21.7
c-Pentyl-	95.6	1.45	20.34	271	10.80	10	−28.4
$CF_3C{\equiv}C$-	*135.4*[a]	−0.77[a]	36.56	413	−9.19	1	32.7
n-HexylC≡C-	*131.0*[a]	0.36	34.31	413	−5.81	1	25.0
$Me_3SiC{\equiv}C$-	*131.6*[a]	0.27	37.50	413	−9.09	1	28.8
$Me_3CC{\equiv}C$-	*131.4*[a]	0.31	34.94	413	−6.49	1	26.1
PhC≡C-	*133.2*[a]	0.43	34.85	413	−6.28	1	27.6
p-CF_3phenylC≡C-	*127.8*[a]	−0.05	36.01	413	−7.91	1	23.9
p-MeOphenylC≡C-	*122.7*[a]	0.28	35.83	413	−7.41	1	18.3
Mesityl-	89.4	0.16	22.19	303	7.31	9	−31.1
-$CH_2C(O)CH_3$	96.0	0.97	26.67	303	3.64	6	−20.5
-CH_2O^tBu	93.0	0.66	25.70	303	4.30	3	−23.8
-CH_2OCH_3	96.1	0.34	26.31	303	3.37	6	−20.2
-CH_2F	101.3	0.03	28.75	340	0.22	3	−11.4
-CHF_2	103.2	−0.26	30.95	373	−2.63	2	−6.4
-CH_2CF_3	106.7	0.91	25.95	303	4.30	3	−10.1

Terminal C–H bond strengths *in italics* for alkynes were calculated using DFT; B3LYP/6-31g**
[a]Energies are in kcal mol^{-1}

of strengths for the substituted methyl derivatives is also "stretched out" for L = PMe_3 vs. L = CNneopentyl.

These trends can also be calculated using DFT and the full [Tp′Rh(PMe_3)] fragment as the model. The results are shown in Fig. 6. Two nearly parallel lines are seen, with the substituted methyl derivatives lying about 12 kcal/mol higher than the hydrocarbons. As before, the slopes by DFT show about 12–13% variance with experiment. The calculated slope for the hydrocarbons is too large, whereas the calculated slope for the substituted methyl derivatives is too small.

The larger slopes for L = PMe_3 vs. L = CNneopentyl indicate that the range of Rh–C bond strengths for the σ-donor complex is larger than for the π-acceptor complex. This has the experimental ramification that the weakest complexes with L = PMe_3 appear less stable than with L = CNneopentyl and that the strongest complexes with L = PMe_3 appear much more stable than with L = neopentyl. For example, Tp′Rh(CNneopentyl)(*n*-pentyl)H loses pentane with a half-life of about 1 h at 30°C, whereas Tp′Rh(PMe_3)(*n*-pentyl)H loses pentane with a half-life of about 30 min at only 9°C. Likewise, loss of phenylacetylene from Tp′Rh (CNneopentyl)(C≡CPh)H occurs with a half-life of about 74 h at 100°C, compared with 60 h at 140°C for Tp′Rh(PMe_3)(C≡CPh)H, a much more difficult elimination.

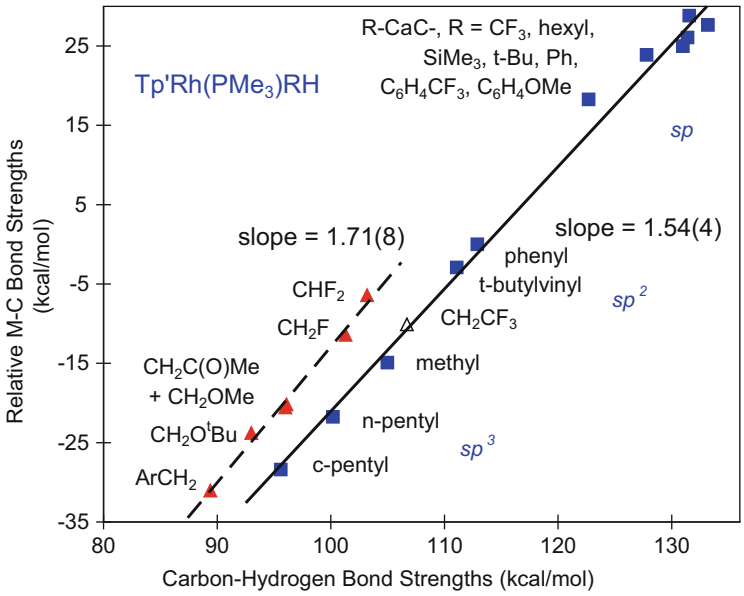

Fig. 5 Plot of relative experimental M–C bond strengths vs. C–H bond strengths for Tp′Rh(PMe_3)(R)H. The *solid line* is fit to the α-unsubstituted hydrocarbons (*blue filled box*, $y = 1.543x - 175.3$), and the *dashed line* is fit to the $–CH_2X$ substrates and $–CHF_2$ (*red filled triangle*, $y = 1.712x - 184.1$). $–CH_2CF_3$ is also shown but not included in either fit. Experimental C–H bond strengths were used for all substrates except the alkynes. Alkyne C–H bond strengths were calculated (B3LYP) since experimental values are unavailable [13]. The vertical separation of the lines at $D_{C–H} = 100$ kcal mol^{-1} is 8.1 kcal mol^{-1}. Reproduced with permission of the ACS from Jiao et al. [18]

6 Hydrocarbon Activation by [Tp′Rh(P(OMe)$_3$)]

As a third test of the effect of the ancillary or "spectator" ligand on the strength of the metal–carbon bond, we set out to use trimethylphosphite as the ligand. Trimethylphosphite is in between trimethylphosphine and neopentylisocyanide in donor/acceptor strength [19], and therefore, we predicted that the slope for the corresponding range of bond strengths should lie in between those found above. As with the PMe_3 series of compounds, two approaches were examined for the formation of the {Tp′Rh[P(OMe)$_3$]} fragment.

One approach uses Tp′Rh[P(OMe)$_3$]H_2 (**7**) as a photochemical precursor of the fragment, and the second uses Tp′Rh[P(OMe)$_3$]MeH (**8**) as the precursor [20]. As in the case with L = PMe_3, irradiation of **7** in hydrocarbon solvents gave the desired products but also showed evidence of several side products. The use of the thermal precursor showed improved product selectivity, and therefore, this was chosen as the route for preparing hydrocarbon activation products. As in the case of PMe_3, the activation of THF solvent during the preparation of **8** led to the formation of some Tp′Rh[P(OMe)$_3$](tetrahydrofuranyl)H in the solution containing **8**, but both served

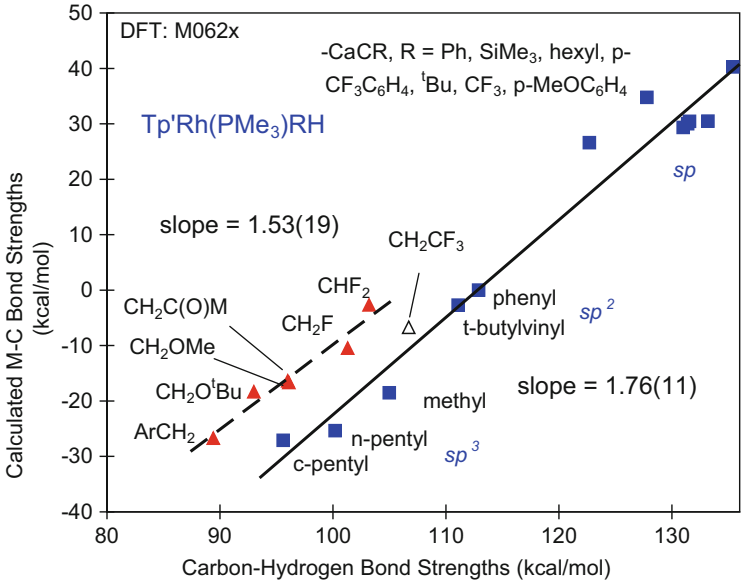

Fig. 6 DFT-calculated plot of relative M–C bond strengths vs. C–H bond strengths for Tp′Rh(PMe_3)(R)H. The *lower line* is fit to the hydrocarbons (*blue filled box*, $y = 1.531x - 162.9$), and the *upper line* is fit to the $-CH_2X$ and CHF_2 substrates (*red filled triangle*, $y = 1.756x - 198.0$). Data for CH_3CF_3 activation is also shown, but not included in the fits. M062X method and basis set 6–31g** for first row atoms and pseudopotentials, additional functions optimized by Stuttgart group for atoms beyond the second row. Experimental C–H bond strengths were used for all substrates except the alkynes. Alkyne C–H bond strengths were calculated (B3LYP) since experimental values are unavailable [13]. The vertical separation of the lines at $D_{C-H} = 100$ kcal mol^{-1} is 12.6 kcal mol^{-1}. Reproduced with permission of the ACS from Jiao et al. [18]

as efficient thermal precursors for {Tp′Rh[$P(OMe)_3$]}. Several hydrocarbon activation products were observed by exchange for methane in **8** (Scheme 4). In the alkyne activations, no evidence was seen for the formation of alkyne π-complexes, again pointing to the need for a strong σ-donor to be present to stabilize the η^2-ligation. In addition, the activation of pentane using **8** was unsuccessful, giving only decomposition after several hours. Instead, Tp′Rh[$P(OMe)_3$](*n*-pentyl)H was prepared by irradiation of **7** in pentane at 10°C. Also, attempted activation of cyclopentane, CH_3CF_3, and CH_2F_2 was unsuccessful, giving only small quantities of the desired products (not enough for use in kinetic studies).

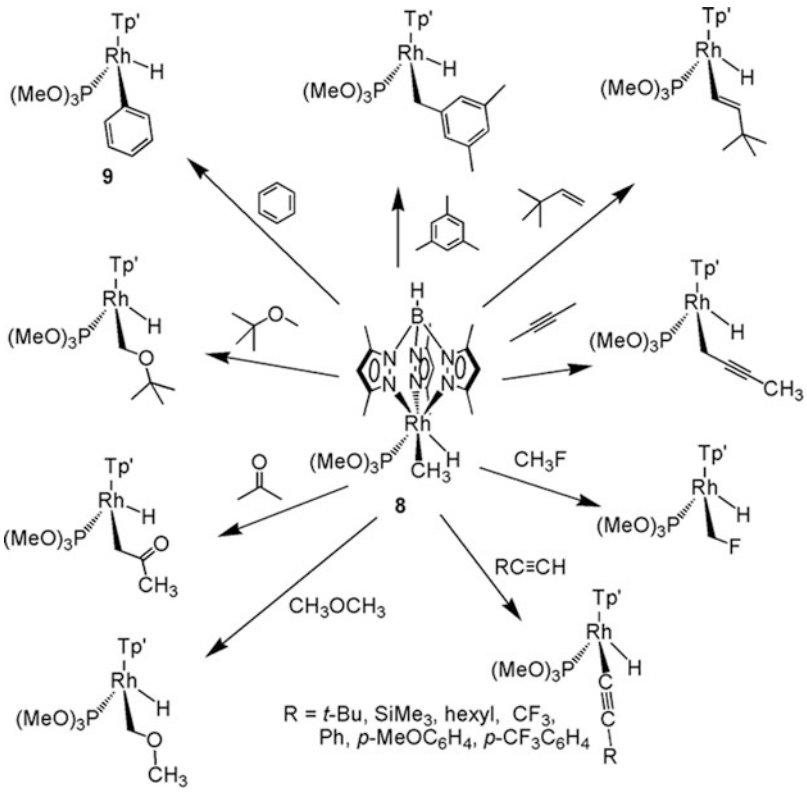

Scheme 4 Reactions of Tp′Rh[P(OMe)$_3$] with hydrocarbon substrates

7 Thermodynamic Determination of Rhodium–Carbon Bond Strengths in Tp′Rh[P(OMe)$_3$](R)H

As with the other ligands, reductive elimination studies were carried out in C_6D_6 solvent to generate hydrocarbon and Tp′Rh[P(OMe)$_3$](C_6D_5)D (**9-*d*$_6$**). The eliminations were carried out at temperatures between 20 and 140°C. To compare these elimination barriers with those of benzene, reductive elimination of C_6H_6 from **9** was carried out at 70–100°C and activation parameters measured for the reductive elimination. An Eyring plot gave $\Delta H^{\ddagger} = 30.7(6)$ kcal/mol and $\Delta S^{\ddagger} = 10.3(3)$ e.u. and permitted comparison of barriers in Fig. 1 at the same temperature. Table 3 summarizes the barrier heights measured and the temperature at which they were measured.

Competition experiments between benzene and the hydrocarbon substrates were examined by photolysis of **7** in a mixture of the two substrates as solvent. Examination of the NMR spectra after a short irradiation time provided the competition data, typically by examination of the area of the hydride resonances of the products.

Table 3 Kinetic and Thermodynamic data for Tp′Rh[P(OMe)$_3$](R)H complexes

R	D(C–H)[a]	$\Delta\Delta G_{oa}^{\ddagger}$ vs. PhH	$\Delta G_{re}^{\ddagger}$	T_{re}(R–H)	ΔG^0 vs. PhH	#H	D_{rel}(M–C)
Ph-	112.9	0	27.61	303	0.01	6	0.0
t-Butylvinyl-	111.1	1.10	27.20	303	1.51	1	−2.3
Methyl-	105.0	0.22	22.64	303	5.20	4	−12.9
n-Pentyl-	100.2	0.67	21.24	298	7.10	6	−19.8
$CF_3C{\equiv}C$-	*135.4*[a]	−0.81	35.01	413	−9.33	1	32.9
n-HexylC≡C-	*131.0*[a]	0.80	35.86	413	−8.57	1	27.7
$Me_3SiC{\equiv}C$-	*131.6*[a]	0.68	36.74	413	−9.58	1	29.3
t-ButylC≡C-	*131.4*[a]	0.89	36.85	413	−9.47	1	29.0
PhC≡C-	*133.2*[a]	0.19	36.63	413	−9.95	1	31.3
p-CF_3phenylC≡C-	*127.8*[a]	0.10	36.25	413	−9.67	1	25.6
p-MeOphenylC≡C-	*122.7*[a]	0.56	35.40	413	−8.35	1	19.2
α-Mesityl-	89.4	0.32	21.86	293	6.18	9	−29.9
-$CH_2C(O)CH_3$	96.0	0.54	25.39	303	2.77	6	−19.7
-$CH_2C{\equiv}CCH_3$	90.7	0.13	25.98	303	1.77	6	−24.0
-CH_2O^tBu	93.0	0.50	25.53	303	2.59	3	−22.1
-CH_2OCH_3	96.1	−0.25	25.24	303	2.13	6	−18.9
-CH_2F	101.3	−0.16	27.92	340	−0.84	3	−10.4

Terminal C–H bond strengths *in italics* for alkynes were calculated using DFT; B3LYP/6-31g**
[a]Energies are in kcal mol^{-1}

The combination of these competition barriers with the reductive elimination barriers gives relative metal–carbon bond strengths with trimethylphosphite as the ancillary ligand, as summarized in Table 3. A plot of D_{rel}(M–C) vs. D_{C-H} is shown in Fig. 7. Here once again, two parallel trends are seen, one for the parent hydrocarbons and one for the substituted methyl derivatives. The slope for the hydrocarbons is 1.55(4), which is similar to that seen with L = PMe_3 (1.54(4)) but smaller than that seen with L = CNneopentyl (1.38(3)). The slope for the substituted methyl derivatives is in between that seen with L = PMe_3 (1.71(8)) and L = CNneopentyl (1.46(19)). Therefore, the effect of the ancillary ligand on rhodium–carbon bond strengths parallels directly the donor ability of the ligand. The better the donor, the wider is the range of metal–carbon bond strengths.

Figure 8 shows the DFT-calculated version of bond strength trends for Tp′Rh[P(OMe)$_3$](R)H complexes. As with the previous two cases, the slopes of the lines are overestimated by about 10%. Does this mean that DFT calculations may be expected to also overestimate the slope in other metal systems? Eisenstein and Perutz made a series of such calculations for both Ti(R)(silox)$_2$(NHSi*t*-Bu$_3$) (silox = OSi*t*-Bu$_3$) and the simplified TpRh(CNMe)(R)H systems [21]. For both systems, about a dozen substrates were considered, and lines were produced with slopes of 1.08 and 1.22, respectively. However, both of these correlations included data for α-mesityl and allyl, and these data can be seen to lie above the correlation for the parent hydrocarbons. From the current studies, we now know why these data

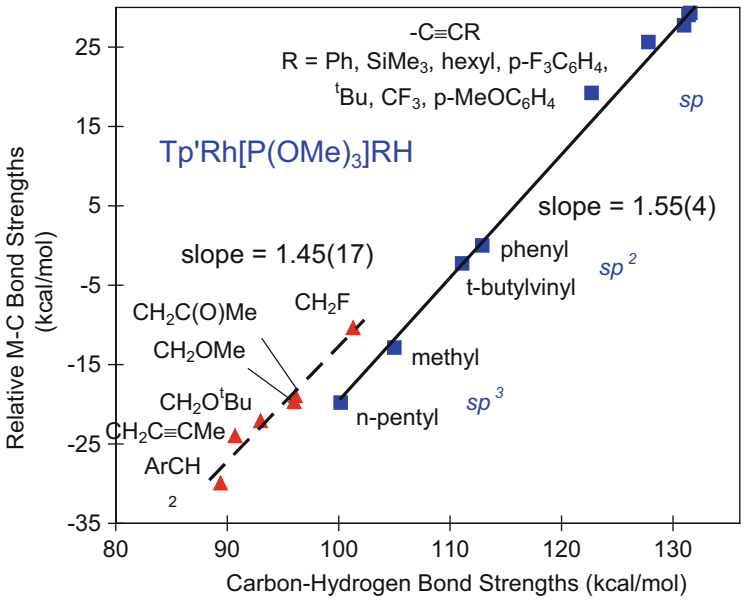

Fig. 7 Plot of relative Rh–R bond strength in Tp′Rh[P(OMe)$_3$](R)H vs. C–H bond strength of hydrocarbon substrates. Experimentally determined D(Rh–C) vs. D(C–H). The *solid line* is fit to the hydrocarbons (*blue filled box*, $y = 1.5501x - 174.59$), and the *dashed line* is fit to the –CH_2X substrates (*red filled triangle*, $y = 1.4535x - 158.06$). Experimental C–H bond strengths were used for all substrates except the alkynes. Alkyne C–H bond strengths were calculated (B3LYP) since experimental values are unavailable [13]. The vertical separation of the lines at $D_{C-H} = 100$ kcal/mol is 6.9 kcal/mol. Reproduced with permission of the RSC from Jiao et al. [20]

lie where they do. Recalculation of the Eisenstein and Perutz data without these points gives revised slopes of 1.33 and 1.71, respectively. The latter is about 24% higher than seen in Fig. 3 (slope = 1.39) and even higher by 7% than the DFT-calculated data seen in Fig. 4 (1.59). This difference between calculated slopes obtained by Eisenstein could be due to either use of a different functional (B3PW91 vs. MO62X) or use of a simplified model or both. The data for the titanium plot also included data for benzyl and methallyl. Removal of these data points gives a slope of 1.33 for the DFT-calculated bond strengths (B3PW91) vs. a slope of 1.35 for experiment, indicating very good agreement. Therefore, DFT can serve as a useful predictor of M–C bond trends, within the above limits.

Furthermore, the observation for all three ligands (PMe_3, $P(OMe)_3$, and CNneopentyl) of a vertical offset for substituted methyl derivatives of about 7 kcal/mol suggests this "additional" bond strength for these ligands might apply generally to other metal complexes. As seen with the data mentioned above by Wolczanski, the substituted methyl data points do indeed lie above the line joining hydrocarbons [22]. Data by Marks for Cp*$_2$Th(R)Cl also show α-benzyl to be an outlier from the trend of six other hydrocarbons [23]. Holland calculated a series of Fe–C bond strengths in (diimine)FeR complexes and found a good linear trend for

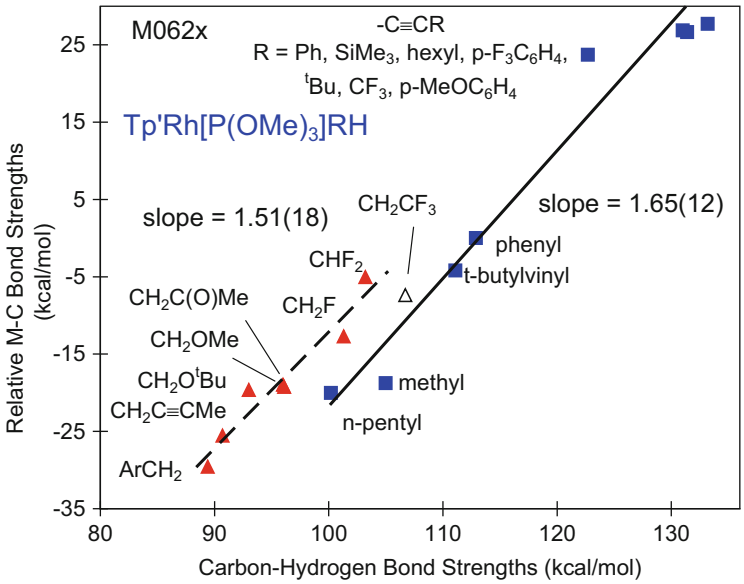

Fig. 8 DFT-calculated D(Rh–C) vs. D(C–H). The *solid line* is fit to the hydrocarbons (*blue filled box*, $y = 1.6527x - 187.02$), and the *dashed line* is fit to the $–CH_2X$ substrates and $–CHF_2$ (*red filled triangle*, $y = 1.508x - 162.94$). Also shown is $–CH_2CF_3$ (*open triangle*) which is not included in either fit. M062X method and basis set 6–31g** for first row atoms and pseudopotentials, additional functions optimized by Stuttgart group for atoms beyond the second row. Experimental C–H bond strengths were used for all substrates except the alkynes. Alkyne C–H bond strengths were calculated (B3LYP) since experimental values are unavailable [13]. The vertical separation of the lines at $D_{C–H} = 100$ kcal/mol is 9.6 kcal/mol. Reproduced with permission of the RSC from Jiao et al. [20]

alkyls [24]. The calculated Fe–C bond strength for $–CH(CH_3)Ph$, however, was found to lie significantly above the line. Landis also calculated relative metal–carbon bond strengths for a series of $H_nM–R$ complexes where R = Me, Et, ^{i}Pr, ^{t}Bu, CH_2F, vinyl, and C≡CH. For 27 different metals (Sc–Au), he observed slopes for M–C vs. C–H plots in the range 1.2–1.9 [25].

Eisenstein and Perutz calculated slopes for fluoroarene activation in [CpRe(CO)L], [CpRhL], and [CpIrL] (L = CO, PH_3) that were 10–20% larger for L = PH_3 than for L = CO [26]. These calculations are in good agreement with the experimental effects seen here for exchange of CNR by PMe_3.

Two other studies worth mentioning here involve the activation of polyfluorinated benzenes $C_6H_nF_{6-n}$ with [Tp′RhL] precursors where L = CNneopentyl or PMe_3. In these reports, a linear correlation is seen between $D_{rel}(M–Ar^F)$ and $D_{ArF–H}$ [15, 27]. However, the slopes observed are 2.14 and 2.15, respectively. Here, replacement of CNneopentyl by PMe_3 appears to have no effect on the range of Rh–C bond strengths. The range of C–H bond strengths spans only 1.5 kcal mol^{-1}, so perhaps the range is too small to see a meaningful trend.

8 Conclusions

This chapter presented studies of C–H activation of sp, sp^2, and sp^3 hybridized carbon containing substrates by reactive [Tp′RhL] precursors (L = CNneopentyl, PMe_3, $P(OMe)_3$). By using the relationship between the kinetics of hydrocarbon reductive elimination and the competition for C–H activation, the thermodynamics for the various activations could be determined. Knowledge of the driving force for a reaction (ΔG^0) allows the determination of the relative rhodium–carbon bond energy. Examination of the trends in M–C bond strength showed four important features.

First, for the parent hydrocarbons (alkanes, alkenes, alkynes), there is a linear relationship between the rhodium–carbon bond strength and the strength of the carbon–hydrogen bond being broken. Second, the range of rhodium–carbon bond strengths exceeds the range of carbon–hydrogen bond strengths by 38–55% depending on the spectator L ligand, resulting in a slope for this linear correlation that is greater than one. This is consistent with a product-driven equilibrium. Third, for substituted methyl derivatives (i.e., Rh–CH_2X, X = F, Cl, CN, OR, Ph, vinyl, keto), the Rh–C bond is about 7 kcal/mol stronger than what would be expected based upon the C–H bond being broken. This "extra" bond strength was attributed to an increase in the ionic character of the metal–carbon bond. Fourth, it was found that a σ-donating L ligand increases the slope of the M–C/C–H correlation, whereas π-acceptors decrease this slope.

Finally, DFT calculations of these same systems with the same substrates show good agreement with the experimentally observed trends. For these systems, however, the DFT calculations overestimate the slopes of the correlations by about 10–12%.

Acknowledgment We thank the U.S. Department of Energy, grant FG02-86ER13569, for their support of this work.

References

1. Hessell ET, Jones WD (1992) Organometallics 11:1496
2. Blaha JP, Dewan JC, Wrighton MS (1986) Organometallics 5:899
3. Bradley MG, Roberta DA, Geoffroy GL (1981) J Am Chem Soc 103:379
4. Geoffroy GL, Bradley MG (1978) Inorg Chem 17:2410
5. Klahn-Oliva AH, Sineer RD, Sutton D (1986) J Am Chem Soc 108:3107
6. Ghosh CK, Graham WAG (1987) J Am Chem Soc 109:4126
7. Jones WD, Hessell ET (1992) J Am Chem Soc 114:6087
8. Jones WD, Hessell ET (1993) J Am Chem Soc 115:554
9. Jones WD, Wick DD (1999) Organometallics 18:495
10. Wick DD, Northcutt TO, Lachicotte RJ, Jones WD (1998) Organometallics 17:4484
11. Northcutt TO, Wick DD, Vetter AJ, Jones WD (2001) J Am Chem Soc 123:7257
12. Wick DD, Reynolds KA, Jones WD (1999) J Am Chem Soc 121:3974

13. Choi G, Morris J, Brennessel WW, Jones WD (2012) J Am Chem Soc 134:9276
14. Jiao Y, Evans ME, Morris J, Brennessel WW, Jones WD (2013) J Am Chem Soc 135:6994
15. Evans ME, Burke CL, Yaibuathes S, Clot E, Eisenstein O, Jones WD (2009) J Am Chem Soc 131:13464
16. Wick DD, Jones WD (2009) Inorg Chim Acta 362:4416
17. Paneque M, Perez PJ, Pizzano A, Poveda ML, Taboada S, Trujillo M, Carmona E (1999) Organometallics 18:4304
18. Jiao Y, Morris J, Brennessel WW, Jones WD (2013) J Am Chem Soc 135:16198
19. Tolman CA (1977) Chem Rev 77:313
20. Jiao Y, Brennessel WW, Jones WD (2014) Chem Sci 5:804
21. Clot E, Mégret C, Eisenstein O, Perutz RN (2006) J Am Chem Soc 128:8350
22. Bennett JL, Wolczanski PT (1997) J Am Chem Soc 119:10696
23. Schock LE, Marks TJ (1988) J Am Chem Soc 110:7701
24. Vela J, Vaddadi S, Cundari TR, Smith JM, Gregory EA, Lachicotte RJ, Flaschenriem CJ, Holland PL (2004) Organometallics 23:5226
25. Uddin J, Morales CM, Maynard JH, Landis CR (2006) Organometallics 25:5566
26. Clot E, Mégret C, Eisenstein O, Perutz RN (2009) J Am Chem Soc 131:7817
27. Tanabe T, Brennessel WW, Clot E, Eisenstein O, Jones WD (2010) Dalton Trans 10495